

General three-dimensional thermal illusion metamaterials

Tianfeng Liu(刘天丰)^{1,2}, Zhaochen Wang(王兆宸)², Zhan Zhu(朱展)², and Run Hu(胡润)^{1,2,†}

¹China-EU Institute for Clean and Renewable Energy, Huazhong University of Science and Technology, Wuhan 430074, China

²School of Energy and Power Engineering, Huazhong University of Science and Technology, Wuhan 430074, China

(Received 28 September 2023; revised manuscript received 23 October 2023; accepted manuscript online 4 November 2023)

Thermal illusion aims to create fake thermal signals or hide the thermal target from the background thermal field to mislead infrared observers, and illusion thermotics was proposed to regulate heat flux with artificially structured metamaterials for thermal illusion. Most theoretical and experimental works on illusion thermotics focus on two-dimensional materials, while heat transfer in real three-dimensional (3D) objects remains elusive, so the general 3D illusion thermotics is urgently demanded. In this study, we propose a general method to design 3D thermal illusion metamaterials with varying illusions at different sizes and positions. To validate the generality of the 3D method for thermal illusion metamaterials, we realize thermal functionalities of thermal shifting, splitting, trapping, amplifying and compressing. In addition, we propose a special way to simplify the design method under the condition that the size of illusion target is equal to the size of original heat source. The 3D thermal illusion metamaterial paves a general way for illusion thermotics and triggers the exploration of illusion metamaterials for more functionalities and applications.

Keywords: thermal illusion, thermal metamaterials, transformation thermotics

PACS: 44.10.+I, 61.46.-w, 07.20.-n

DOI: 10.1088/1674-1056/ad09aa

1. Introduction

Mirage is one of the most well-known optical illusions in nature, which is formed by a curved light path in inhomogeneous air with varying density. Inspired by natural optical illusions, people have designed numerical optical metamaterials^[1–3] or metasurfaces to create artificial, specific, targeted optical illusions for conformal mapping,^[4] shear polaritons,^[5] remote cooling,^[6] and so on. Similarly, thermal illusions^[7–15] aim at creating fake thermal signals or hiding the thermal target from the background thermal field to mislead infrared (IR) observers for some military applications. As all objects emit thermal energy externally, they can be easily observed by IR cameras even in gloomy and dark environment. According to the Stefan–Boltzmann’s law, the emitted thermal energy is proportional to the fourth power of temperature and surface emissivity, thus the temperature plays a more important role than the surface emissivity in quantifying the emitted thermal energy.^[16–20] Obeying the second law of thermodynamics, thermal energy flows from the high-temperature region to the low-temperature region spontaneously, and manipulating the surface temperature field for thermal illusion is rather challenging.^[20–22] To achieve this, Hu *et al.* proposed the heuristic and inspiring concept of illusion thermotics,^[8,13,14] which is the first to deal with heat sources in a thermal field by splitting the heat sources and simultaneously creating several separate thermal illusions to camouflage the practical heat sources. However, previous studies^[8,9,14] only deal with 2D illusion thermotics, and more

general 3D cases have remained unresolved.

Note that both the 2D and 3D thermal illusion metamaterial designs employ the general transformation thermotics,^[23–34] whose essence lies in the invariance of the thermal conduction differential equation after space transformation. In 3D space, thermal conduction is governed by $\rho(x, y, z, t) c(x, y, z, t) \frac{\partial T}{\partial t} = \nabla \cdot (k(x, y, z, t) \nabla T)$. After space transformation $(x, y, z) \rightarrow (x'(x, y, z), y'(x, y, z), z'(x, y, z))$, the governing equation can be rewritten as $\rho(x', y', z', t) c(x', y', z', t) \frac{\partial T}{\partial t} = \nabla \cdot (\mathbf{J}k(x, y, z, t) \mathbf{J}^{-T} / \det(\mathbf{J}) \nabla T)$, where the transformation Jacobin matrix $\mathbf{J} = \partial(x', y', z') / \partial(x, y, z)$. Compare the two equations above and we can get the effective thermal conductivity tensor in 3D space as $\mathbf{k}' = \mathbf{J}k(x, y, z, t) \mathbf{J}^{-T} / \det(\mathbf{J})$. Following this design framework, we need to set up the design domain, the coordinates of the original heat sources and the separate thermal illusions, and set up the space dividing methods to apply the coordinate transformation method. To design 2D thermal illusion metamaterials, Fig. 1(a) shows a red-colored man (the real heat source) at the center of the 2D temperature field without any illusion device. And in Fig. 1(b), when a 2D illusion device is applied, the red man is expected to move to the location of the blue man (the virtual heat source). Figures 1(c) and 1(d) extend this effect from 2D to 3D. It is worth noting that the division of 2D space regions doesn’t have a great impact on the position of illusion while in a 3D illusion device, if the region is not elaborately divided, the expected illusion target blue man won’t appear, instead

[†]Corresponding author. E-mail: hurun@hust.edu.cn

the gray man at the wrong position appears. As shown in Fig. 2(c), both the heat source (or the illusion target) and the box outside are hexahedrons, and each of them has 8 vertices. If we connect these vertices randomly, the regional division will be messy and we can not get a general 3D illusion model. Shifting from 2D to 3D is not just a simple addition of dimension but a complicated work. Therefore, it remains to be studied how the 3D region should be divided and what diverse functionalities it may present.

In this study, we propose a general design framework to design 3D thermal illusion metamaterials to manipulate thermal illusions at arbitrary size and position. To demonstrate the generality, different thermal functionalities of thermal shifting, splitting, trapping, amplifying and compressing have been realized. A way to simplify our model is when the size of the illusion target is equal to the size of the original heat source. The 3D thermal illusion metamaterial offers a general way for illusion thermotics and promotes the further exploration of illusion metamaterials for more functionalities and practical ap-

plications.

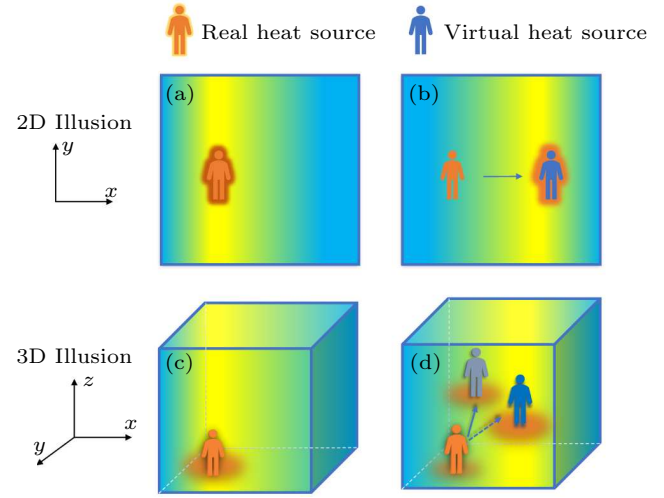


Fig. 1. Schematic of 2D and 3D thermal illusions. (a) 2D reference temperature field. (b) 2D thermal illusion metadvice. (c) 3D reference temperature field. (d) 3D thermal illusion metadvice.

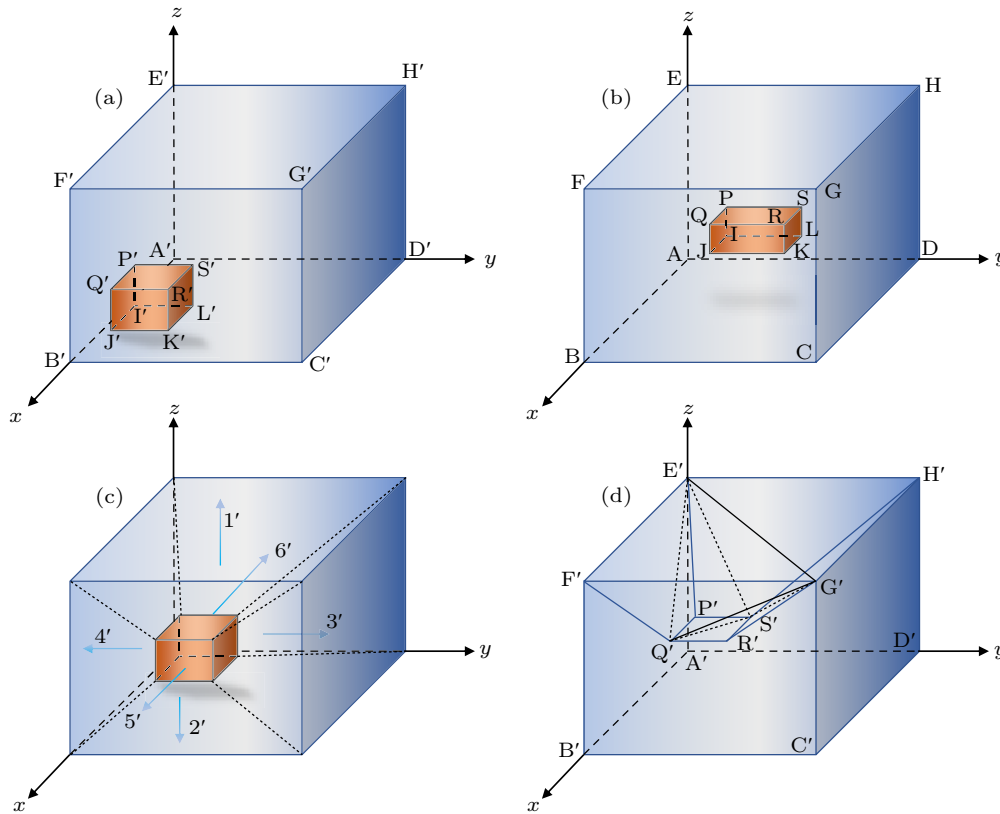


Fig. 2. Schematic of the 3D thermal illusion design. (a) Schematic of original heat source in the real space. (b) Schematic of thermal illusion target in the virtual space. (c) Schematic of space divided into six hexahedral regions. (d) Schematic of hexahedral region 1 divided into five tetrahedron regions.

2. Methods

As is shown in Figs. 2(a) and 2(b), located in the 3D Cartesian coordinate system, the original hexahedral target $I'J'K'L'P'Q'R'S'$ in the real space box $A'B'C'D'E'F'G'H'$ is expected to be transferred to the illusion hexahedral target box

$IJKLPQRS$ in the virtual space $ABCDEFGH$. The coordinate transformation is performed within the box, so the real box and virtual box share the same dimension size of $t \times w \times h$. The original target and the illusion target separately have the dimension sizes of $l \times m \times n$ and $ll \times mm \times nn$. For simplified calculation, we put A' and A at the origin of the real and

virtual space coordinates, and we set $A'B'$ and AB as the positive direction of the x axis, $A'C'$ and AC as the positive direction of the y axis, and $A'E'$ and AE as the positive direction of the z axis. Besides, in order to represent the movement of objects in space, we set the coordinates of the point I' to be (p, q, r) and I to be (pp, qq, rr) . To avoid confusion, only the method of dividing regions in the real space is introduced, while in the virtual space with the same dividing principle we just need to remove the superscript of the real space results. Broadly, we divide the region outside the original target into six hexahedral regions, with each hexahedral region further divided into five tetrahedral regions. As is shown in Fig. 2(c), the hexahedral regions above ($E'F'G'H'P'Q'R'S'$) and below ($A'B'C'D'I'J'K'L'$) the target are named region 1' and region 2', respectively. The hexahedral regions in front ($B'C'G'F'J'K'R'Q'$) and back ($A'D'H'E'I'L'S'P'$) of the target are named region 3' and region 4'. The hexahedral regions on the right ($D'C'G'H'L'K'R'S'$) and left ($A'B'F'E'I'J'Q'P'$) of the target are named region 5' and region 6'. Taking region 1' for example, we further divide the hexahedral region into five tetrahedral regions, as is shown in Fig. 2(d), and they are $E'P'Q'S'$, $G'R'Q'S'$, $Q'E'G'F'$, $S'E'G'H'$ and $E'S'Q'G'$, which are named region 1.1', region 1.2', region 1.3', region 1.4' and region 1.5', respectively. The residual hexahedral regions are divided in the same order.

According to the coordinate transformation relationship, each point (x, y, z) in each tetrahedral region in the virtual space can be mapped to new a one (x', y', z') in the corresponding tetrahedral region in the real space by the following linear relationship:

$$\begin{pmatrix} x'_n \\ y'_n \\ z'_n \end{pmatrix} = \begin{pmatrix} \alpha_n & \beta_n & \gamma_n & \varphi_n \\ \mu_n & \nu_n & \varepsilon_n & \theta_n \\ \lambda_n & \sigma_n & \rho_n & \omega_n \end{pmatrix} \begin{pmatrix} x_n \\ y_n \\ z_n \\ 1 \end{pmatrix}, \quad (1)$$

where the subscript n denotes the sequence number of the tetrahedral region. Then the Jacobian matrix and the effective conductivity tensor can be written as

$$\mathbf{J}_n = \frac{\partial(x', y', z')}{\partial(x, y, z)} = \begin{pmatrix} \alpha_n & \beta_n & \gamma_n \\ \mu_n & \nu_n & \varepsilon_n \\ \lambda_n & \sigma_n & \rho_n \end{pmatrix}, \quad (2)$$

$$\mathbf{k}'_n = \begin{pmatrix} k'_{xx} & k'_{xy} & k'_{xz} \\ k'_{yz} & k'_{yy} & k'_{yz} \\ k'_{zx} & k'_{zy} & k'_{zz} \end{pmatrix} = \frac{\mathbf{J}_n \mathbf{k}_0 \mathbf{J}_n^T}{\det(\mathbf{J}_n)}, \quad (3)$$

where k_0 denotes the thermal conductivity of the virtual space.

Firstly we need to correspond each point in the real space region to the virtual space region. As each point represents three axial coordinates, then twelve equations can be formed in each tetrahedral region, and twelve coefficients in Eq. (1) can be solved, but we just need the left three columns of the Jacobian matrix which are indicated in Eq. (2). Here we only

give the detailed derivation of thermal conductivity tensors of region 1.

Table 1. Coefficients of tetrahedron region from region 1.1 to region 1.3.

Region	1.1	1.2	1.3
α	$\frac{l}{ll}$	$\frac{l}{ll}$	1
β	0	0	0
γ	$-\frac{llp-lpp}{ll(h-nn-rr)}$	$-\frac{llp-lpp+lr-llt}{ll(h-nn-rr)}$	$-\frac{l-ll+p-pp}{h-nn-rr}$
φ	$\frac{h(llp-lpp)}{ll(h-nn-rr)}$	$-\frac{h(llp-llp)+t(nn+rr)(ll-l)}{ll(h-nn-rr)}$	$\frac{h(l-ll+p-pp)}{h-nn-rr}$
μ	0	0	0
ν	$\frac{m}{mm}$	$\frac{m}{mm}$	1
ε	$-\frac{mmq-mqq}{mm(h-nn-rr)}$	$-\frac{mmq-mqq+mw-nmw}{mm(h-nn-rr)}$	$-\frac{q-qq}{h-nn-rr}$
θ	$\frac{h(mmq-mqq)}{mm(h-nn-rr)}$	$-\frac{h(mmq-mmq)+w(rr+nn)(mm-m)}{mm(h-nn-rr)}$	$\frac{h(q-qq)}{h-nn-rr}$
λ	0	0	0
σ	0	0	0
ρ	$-\frac{-h+n+r}{h-nn-rr}$	$-\frac{-h+n+r}{h-nn-rr}$	$-\frac{-h+n+r}{h-nn-rr}$
ω	$\frac{h(n-nn+r-rr)}{h-nn-rr}$	$-\frac{-hn+hn-hr+hr}{h-nn-rr}$	$\frac{h(n-nn+r-rr)}{h-nn-rr}$

Table 2. Coefficients of tetrahedron regions 1.4 and 1.5.

Region	1.4	1.5
α	1	$-\frac{mmt-lw}{mmt+llw}$
β	0	$-\frac{(l-ll)t}{mmt+llw}$
γ	$-\frac{p-pp}{h-nn-rr}$	$-\frac{lmt-lmmt+mmt-mmppt+lqqt-llqqt+llpw-lppw}{(h-nn-rr)(mmt+llw)}$
φ	$\frac{h(p-pp)}{h-nn-rr}$	$-\frac{h(-lmmt+llmmt-mmpt+mmppt-lqqt+llqqt-llpw+lppw)}{(h-nn-rr)(mmt+llw)}$
μ	0	$-\frac{mw-mmw}{mmt+llw}$
ν	1	$-\frac{mt-llw}{mmt+llw}$
ε	$-\frac{m-nn+q-qq}{h-nn-rr}$	$-\frac{mmqt-mqqt+llmw-llmmw+mppw-mmppw+llqw-llqpw}{(h-nn-rr)(mmt+llw)}$
θ	$\frac{h(m-nn+q-qq)}{h-nn-rr}$	$\frac{h(mmqt-mqqt+llmw-llmmw+mppw-mmppw+llqw-llqpw)}{(h-nn-rr)(mmt+llw)}$
λ	0	0
σ	0	0
ρ	$-\frac{-h+n+r}{h-nn-rr}$	$-\frac{-h+n+r}{h-nn-rr}$
ω	$\frac{h(n-nn+r-rr)}{h-nn-rr}$	$\frac{h(n-nn+r-rr)}{h-nn-rr}$

As is shown in Fig. 2(d), the coordinates that we need are $E'(0, 0, h)$, $F'(t, 0, h)$, $G'(t, w, h)$, $H'(0, w, h)$, $P'(p, q, r+n)$, $Q'(p+l, q, r+n)$, $R'(p+l, q+m, r+n)$, $S'(p, q+m, r+n)$. According to Eq. (1), we can set the following equations of region 1.3:

$$\begin{pmatrix} p+l & 0 & t & t \\ q & 0 & w & 0 \\ r+n & h & h & h \end{pmatrix} = \begin{pmatrix} \alpha_{1.3} & \beta_{1.3} & \gamma_{1.3} & \varphi_{1.3} \\ \mu_{1.3} & \nu_{1.3} & \varepsilon_{1.3} & \theta_{1.3} \\ \lambda_{1.3} & \sigma_{1.3} & \rho_{1.3} & \omega_{1.3} \end{pmatrix} \begin{pmatrix} pp+ll & 0 & t & t \\ qq & 0 & w & 0 \\ rr+nn & h & h & h \\ 1 & 1 & 1 & 1 \end{pmatrix}. \quad (4)$$

Solving Eq. (4) and we can get the values of all the linear coefficients as $\alpha = 1$, $\beta = 0$, $\gamma = -\frac{l-ll+p-pp}{h-nn-rr}$, $\varphi = \frac{h(l-ll+p-pp)}{h-nn-rr}$, $\mu = 0$, $\nu = 1$, $\varepsilon = -\frac{q-qq}{h-nn-rr}$, $\theta = \frac{h(q-qq)}{h-nn-rr}$, $\lambda = 0$,

$\sigma = 0$, $\rho = -\frac{-h+n+r}{h-nn-rr}$, $\omega = \frac{h(n-nn+r-rr)}{h-nn-rr}$. The other coefficients of each tetrahedron region are listed in Table 1 (including regions 1.1, 1.2 and 1.3) and Table 2 (regions 1.4 and 1.5).

$$\mathbf{k}_{1.3} = \begin{pmatrix} \frac{\left(1 + \frac{(l-ll+p-pp)^2}{(h-nn-rr)^2}\right)(h-nn-rr)}{-h+n+r} & -\frac{(l-ll+p-pp)(q-qq)}{(-h+n+r)(h-nn-rr)} & -\frac{l-ll+p-pp}{h-nn-rr} \\ -\frac{(l-ll+p-pp)(q-qq)}{(-h+n+r)(h-nn-rr)} & \frac{\left(1 + \frac{(q-qq)^2}{(h-nn-rr)^2}\right)(h-nn-rr)}{-h+n+r} & -\frac{q-qq}{h-nn-rr} \\ -\frac{l-ll+p-pp}{h-nn-rr} & -\frac{q-qq}{h-nn-rr} & -\frac{-h+n+r}{h-nn-rr} \end{pmatrix}. \quad (5)$$

Following the same methods, we can derive all the thermal conductivity tensors of all the tetrahedron regions.

3. Results and discussion

Following the above-mentioned methods, we get all the 3D conductivity tensors of the divided tetrahedral regions. Before further study, we find that when the heat source and illusion target have the same size, i.e., $l = ll$, $m = mm$, $n = nn$, five tetrahedral regions divided by the same hexahedral region share the same linear coefficients. Take region 1 for exam-

Then Jacobian matrix of region 1.3 can be obtained and plugged it into Eq. (3), so that we can get the thermal conductivity tensor of region 1.3 as

ple, the coefficients of regions 1.1, 1.2, 1.3, 1.4 and 1.5 are reduced as $\alpha = 1$, $\beta = 0$, $\gamma = \frac{p-pp}{h-rr-nn}$, $\varphi = \frac{h(p-pp)}{h-rr-nn}$, $\mu = 0$, $\nu = 1$, $\varepsilon = \frac{q-qq}{h-rr-nn}$, $\theta = \frac{h(q-qq)}{h-rr-nn}$, $\lambda = 0$, $\sigma = 0$, $\rho = \frac{h-r-n}{h-rr-nn}$, $\omega = \frac{h(r-rr)}{h-rr-nn}$, thereby the Jacobian matrix can be reduced to

$$\mathbf{J}_1 = \begin{pmatrix} 1 & 0 & \frac{p-pp}{h-rr-nn} \\ 0 & 1 & \frac{q-qq}{h-rr-nn} \\ 0 & 0 & \frac{h-r-n}{h-rr-nn} \end{pmatrix}, \quad (6)$$

and thermal conductivity tensor becomes

$$\mathbf{k}_1 = \begin{pmatrix} \frac{(h-n-rr)\left(1 + \frac{(p-pp)^2}{(-h+n+rr)^2}\right)}{-h+n+r} & -\frac{(p-pp)(q-qq)}{(h-n-r)(-h+n+rr)} & \frac{p-pp}{-h+n+rr} \\ -\frac{(p-pp)(q-qq)}{(h-n-r)(-h+n+rr)} & \frac{(h-n-rr)\left(1 + \frac{(q-qq)^2}{(-h+n+rr)^2}\right)}{-h+n+r} & \frac{q-qq}{-h+n+rr} \\ \frac{p-pp}{-h+n+rr} & \frac{q-qq}{-h+n+rr} & \frac{-h+n+r}{-h+n+rr} \end{pmatrix}. \quad (7)$$

In this way, we find a way to simplify the tetrahedral model to the hexahedral model, which greatly reduces the amount of computation. Therefore, in the following study without changing the size of the heat source, we adopt the hexahedral model to show a clearer presentation of the temperature field.

In order to visually present the results, finite element method (FEM) simulation is applied to validate our work. Relevant parameters are set as follows: the dimension of the box is length $t = 100$ mm, width $w = 100$ mm and height $h = 20$ mm. Other variable parameters are given in the corresponding description. In order to be closer to the real environment, all the boundaries are cooled by natural convection with a convection coefficient of $5 \text{ W} \cdot \text{m}^{-2} \cdot \text{K}^{-1}$ and the ambient temperature is set as 293 K. The 3D temperature field of the reference

group shown in Fig. 3(a) has a uniform thermal conductivity, with the temperature field distribution of its bottom surface and top surface. We can easily identify the location of the $10 \text{ mm} \times 10 \text{ mm} \times 2 \text{ mm}$ heat source from the top surface, and that is why we manufacture thermal illusion to mislead and hide the real heat source. Then, based on various means of manufacturing illusions, a series of novel thermal functionalities are designed and simulated.

Thermal shifter As we set the illusion target away from the heat source, the temperature field acts like there is a real object at the illusion position. Technically, as long as we put the heat source and illusion target in different positions, whether there are areas of overlap or not, we will make a thermal illusion shifter. To make this effect more noticeable, we

set the geometrical size of the original heat source and illusion target as length $l = ll = 10$ mm, width $m = mm = 10$ mm, and height $n = nn = 2$ mm. We set the coordinates of point I' as $I'(45, 45, 0)$ and point I as $I(80, 45, 15)$. As is shown in Fig. 3(b), the heat source is shifted to the position of the illusion target.

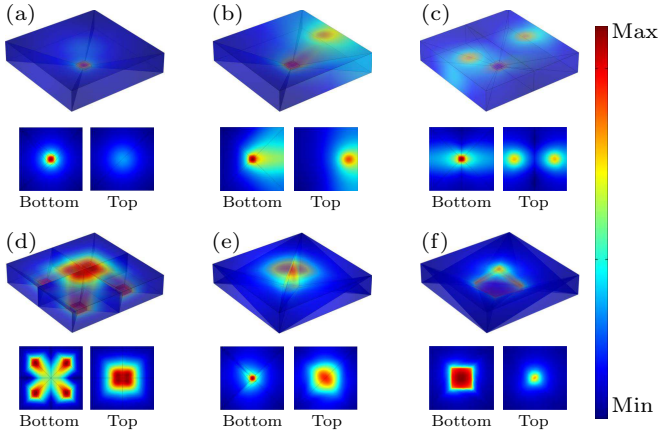


Fig. 3. FEM demonstration of thermal illusion. (a) Reference. (b) Thermal shifter. (c) Thermal splitter. (d) Thermal trapper. (e) Thermal amplifier. (f) Thermal compressor.

Thermal splitter Based on the thermal shifter, if we first set the heat source to the side of the outer box and the illusion target to the center of the box, then we compress the whole box in half in terms of length. Finally, we join together two symmetrical in plane, so that two illusion targets are gained while there exists only one heat source, as is shown in Fig. 3(c). The heat source and illusion target share the same dimension size of length $l = 5$ mm, width $m = 10$ mm and height $n = 2$ mm. The length of each outer box is $t = 50$ mm, the coordinates of point I' to be $I'(0, 45, 0)$ and point I to be $I(27.5, 45, 15)$.

Thermal trapper Contrary to the design logic of the thermal splitter, if we set the illusion target near the corner of the outer box and splice four of them together, we can get one illusion target while there exist four heat sources, as is shown in Fig. 3(d). In our design, each outer box is compressed to the size of $50 \text{ mm} \times 50 \text{ mm} \times 20 \text{ mm}$, while the heat source and illusion target have the dimension size of $10 \text{ mm} \times 10 \text{ mm} \times 4 \text{ mm}$. The common side that all four outer boxes intersect is the z axis. We set I' to be $I'(20, 20, 0)$ and I to be $I(1, 1, 15)$. Here we give the coordinates of the first trigrams, and the coordinates of the other trigrams are symmetric or centrosymmetric.

Thermal amplifier and thermal compressor All the researches above are carried out on the basis of the hexahedron-region model, and when it comes to scaling the size of the illusion target, we will have to adopt the tetrahedral-region model. As is shown in Figs. 3(e) and 3(f), we manage to amplify and shrink the illusion target compared to the original heat source, and we call them thermal amplifier and thermal compressor, respectively. For thermal amplifier, the dimension

size of heat source is length $l = 10$ mm, width $m = 10$ mm and height $n = 2$ mm, and the dimension size of illusion target is length $ll = 30$ mm, width $mm = 30$ mm and height $nn = 2$ mm. For thermal compressor, the dimension size of heat source is length $l = 30$ mm, width $m = 30$ mm and height $n = 2$ mm, and the dimension size of illusion target is length $ll = 5$ mm, width $mm = 5$ mm and height $nn = 2$ mm.

It needs to be stressed that our general 3D thermal illusion model is designed for a fixed heat source, both the location and shape. A structure with a specific function will direct the heat flux at the illusion target, which means that if we move, enlarge or shrink the heat source, the trend of heat flow guidance will not change. However, the desired effect can not be achieved perfectly or proportionably. In addition, the achievement of thermal illusion does not depend on the location of the observer, but observers at different locations may observe differently. As shown in Fig. 3(b), observers above and below the outside space box may observe different temperature fields.

In order to see the temperature distribution more accurately, we intercept the plane where $y = 50$ mm of the reference group, thermal shifter group and thermal amplifier group. $z = 1$ mm and $z = 16$ mm are the center plane of the heat source and illusion target and we define dimensionless temperature as $T^* = \frac{T - T_{\min}}{T_{\max} - T_{\min}}$. Figure 4(a) shows that heat flux is not selective in direction and to break this kind of symmetry, as is shown in Fig. 4(b), heat flux moves to the positive x -axis and peaks at $x = 80$ mm, after which point its value starts to decline. The temperature field fits perfectly with our designed illusion position, which further verifies the reliability of our model. Compared with Fig. 4(a), Fig. 4(c) shows that at $z = 16$ mm, there has a wider area where temperature drops sharply, which indicates that there exists a heat source bigger than that of the original given one.

The variation of thermal conductivity tensor reflects the essence of thermal conduction, so it is necessary to study this constitutive relation. The distance between heat source and illusion target is of vital importance, so we take the z -coordinates of illusion target as argument, i.e., the value of rr . Take thermal shifter group as an example, the three principal components of thermal conductivity tensor (k_{xx} , k_{yy} and k_{zz}) of the six hexahedron regions change with rr are shown in Figs. 5(a)–5(f). From the overall trend, only thermal conductivities of xx direction in regions 1 and 2 change significantly with the change of rr , while the others are not sensitive to the change of rr . In our design, illusion target moves only on segments $(80, 45, 0)$ through $(80, 45, 18)$. So when illusion target is below or above the heat source, the heat flux is mainly regulated by the thermal conductivity in xx direction of region 2 or region 1, and the other regions only play an auxiliary role in heat flux regulation.

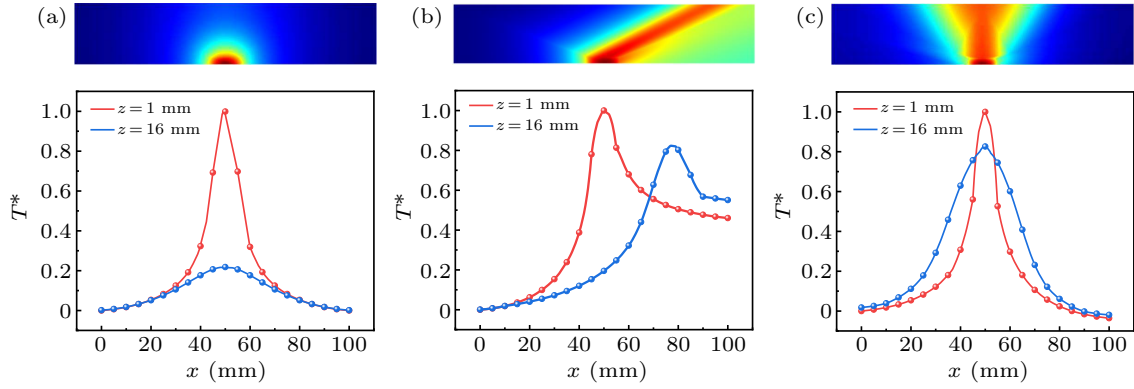


Fig. 4. Temperature distribution. (a) Reference group. (b) Thermal shifter group. (c) Thermal amplifier group.

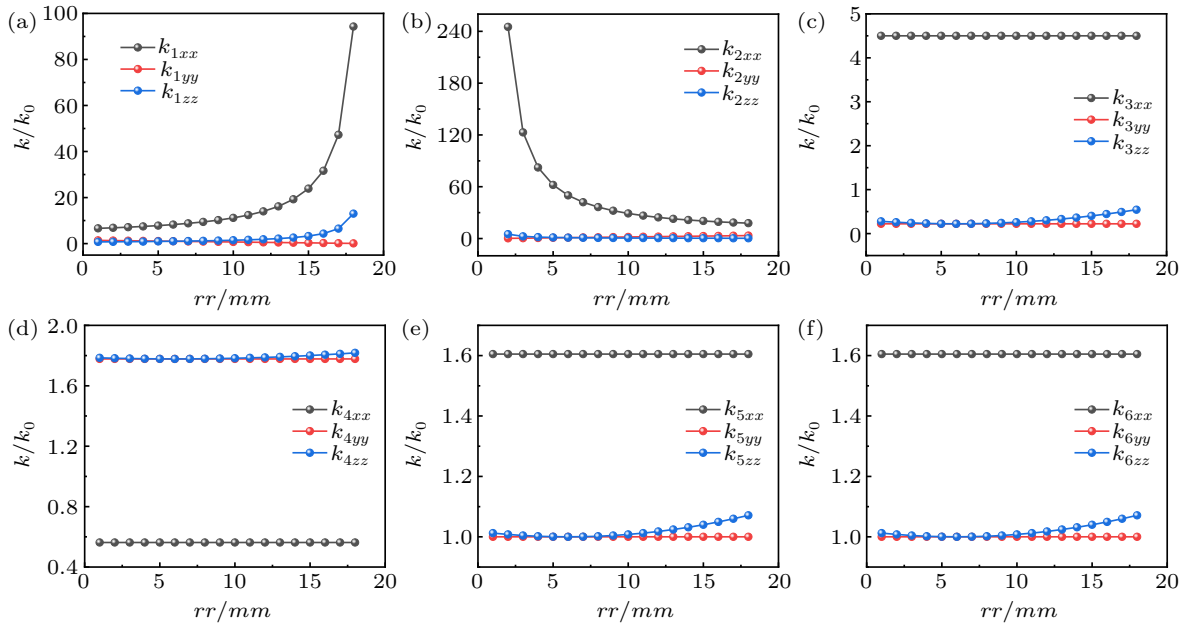


Fig. 5. Three principal components of thermal conductivity tensors of different hexahedron regions on the height of illusion target. Panels (a)–(f) represent regions 1–6, respectively.

4. Conclusion

We propose a general 3D thermal illusion model to achieve functionalities of thermal shifting, splitting, trapping, amplifying and compressing. A general design method has been proposed to divide the design domain and derive the general formula of thermal conductivity tensors of each region under the theory of transformation thermotics. Based on this model, a series of thermal functionalities have been realized. In addition, we find a way to simplify our tetrahedron-region model into a hexahedron-region model under the condition that the size of illusion target equals the size of original heat source. The achievement of thermal illusion does not depend on the location of the observer, but observers at different locations may observe differently. As shown in Fig. 3, observers above and below the outside space box share different temperature fields. The 3D thermal illusion metamaterial paves a general way for illusion thermotics and triggers the exploration of illusion metamaterials for more functionalities and applications.

Acknowledgments

Project supported by the National Natural Science Foundation of China (Grant Nos. 52211540005 and 52076087), the Natural Science Foundation of Hubei Province of China (Grant No. 2023AFA072), the Open Project Program of Wuhan National Laboratory for Optoelectronics (Grant No. 2021WNLOKF004), the Wuhan Knowledge Innovation Shuguang Program, and the Science and Technology Program of Hubei Province of China (Grant No. 2021BLB176).

References

- [1] Pendry J B, Schurig D and Smith D R 2006 *Science* **312** 1780
- [2] Schurig D, Mock J J, Justice B J, Cummer S A, Pendry J B, Starr A F and Smith D R 2006 *Science* **314** 977
- [3] Schurig D, Pendry J B and Smith D R 2006 *Opt. Express* **14** 9794
- [4] Leonhardt U 2006 *Science* **312** 1777
- [5] Jie S, Xue S, Yang Z, Ge Z, Bao Q, Zhu S and Chen H 2023 *Opt. Lett.* **48** 2688
- [6] Sun F and He S 2017 *Sci. Rep.* **7** 40949
- [7] Peng Y, Li Y, Cao P, Zhu X and Qiu C 2020 *Adv. Funct. Mater.* **30** 2002061

- [8] Hu R, Huang S, Wang M, Luo X, Shiomi J and Qiu C 2019 *Adv. Mater.* **31** 1807849
- [9] Chen Y X, Shen X Y and Huang J P 2015 *Eur. Phys. J. Appl. Phys.* **70** 20901
- [10] Han T, Bai X, Thong J T L, Li B and Qiu C W 2014 *Adv. Mater.* **26** 1731
- [11] Hou Q, Zhao X, Meng T and Liu C 2016 *Appl. Phys. Lett.* **109** 103506
- [12] He X and Wu L 2014 *Appl. Phys. Lett.* **105** 221904
- [13] Hu R, Zhou S, Li Y, Lei D Y, Luo X and Qiu C W 2018 *Adv. Mater.* **30** 1707237
- [14] Zhou S, Hu R and Luo X 2018 *Int. J. Heat Mass Transf.* **127** 607
- [15] Peng X and Hu R 2019 *ES Energy Environ.* **6** 39
- [16] Zhang J, Huang S and Hu R 2021 *Chin. Phys. Lett.* **38** 010502
- [17] Liu Y, Song J, Zhao W, Ren X, Cheng Q, Luo X, Fang N X and Hu R 2020 *Nanophotonics* **9** 855
- [18] Liu Y, Zuo H, Xi W, Hu R and Luo X 2022 *Adv. Mater. Technol.* **7** 2100821
- [19] Hu R, Xi W, Liu Y, Tang K, Song J, Luo X, Wu J and Qiu C W 2021 *Mater. Today* **45** 120
- [20] Zhu Z, Ren X, Sha W, Xiao M, Hu R and Luo X 2021 *Int. J. Heat Mass Transf.* **176** 121417
- [21] Sha W, Xiao M, Zhang J, Ren X, Zhu Z, Zhang Y, Xu G, Li H, Liu X, Chen X, Gao L, Qiu C W and Hu R 2021 *Nat. Commun.* **12** 7228
- [22] Sha W, Zhao Y, Gao L, Xiao M and Hu R 2020 *J. Appl. Phys.* **128** 045106
- [23] García-Meca C and Barceló C 2016 *J. Opt.* **18** 044026
- [24] Su Y, Li Y, Yang T, Han T, Sun Y, Xiong J, Wu L and Qiu C 2021 *Adv. Mater.* **33** 2003084
- [25] Fan C Z, Gao Y and Huang J P 2008 *Appl. Phys. Lett.* **92** 251907
- [26] Lei M, Jiang C, Yang F, Wang J and Huang J 2023 *Int. J. Heat Mass Transf.* **207** 124033
- [27] Yang F, Jin P, Lei M, Dai G, Wang J and Huang J 2023 *Phys. Rev. Appl.* **19** 054096
- [28] Hu R, Zhou S, Shu W, Xie B, Ma Y and Luo X 2016 *AIP Adv.* **6** 125111
- [29] Loke D, Skelton J M, Chong T C and Elliott S R 2016 *ACS Appl. Mater. Interfaces* **8** 34530
- [30] Li Y, Shen X, Wu Z, Huang J, Chen Y, Ni Y and Huang J 2015 *Phys. Rev. Lett.* **115** 195503
- [31] Narayana S and Sato Y 2012 *Phys. Rev. Lett.* **108** 214303
- [32] Li J, Gao Y and Huang J 2010 *J. Appl. Phys.* **108** 074504
- [33] Stedman T and Woods L M 2017 *Sci. Rep.* **7** 6988
- [34] Ma Y, Liu Y, Raza M, Wang Y and He S 2014 *Phys. Rev. Lett.* **113** 205501